



Topological design of electrode shapes for dielectrophoresis based devices

Gil Ho Yoon^{a,*}, Jungyul Park^b

^a School of Mechanical Engineering, Kyungpook National University, Daegu, Republic of Korea

^b Mechanical Engineering, Sogang University, Republic of Korea

ARTICLE INFO

Article history:

Received 10 February 2010

Received in revised form

10 June 2010

Accepted 14 June 2010

Available online 4 July 2010

Keywords:

Cell separation

Structural optimization

Dielectrophoresis

Topology optimization

ABSTRACT

This research develops a topology optimization procedure to find out the optimal shapes of electrodes for cell sorter devices based on dielectrophoresis phenomenon which moves dielectrically polarizable particles in the presence of nonuniform electric field. After understanding the working principle of dielectrophoresis based devices mathematically, the spatial distributions of the square electric field is defined as the objective function and it is possible to define an optimization formulation in the framework of the standard topology optimization procedure. To show the potential of the developed procedure, optimized electrodes as well as some illustrative numerical examples are presented.

© 2010 Elsevier B.V. All rights reserved.

1. Introduction

Effective separation and statistical analysis of living cells using bio-microelectromechanical systems (bio-MEMS) is critical in contemporarily molecular biology, drug screening, diagnostics, and cell replacement therapy (CRT). Since more than 90% of the time and cost involved in acquiring molecular diagnostic data is spent on sample preparation, separation, and collection [1,2], many cell separation techniques have been proposed: density gradient centrifugation [3], electrophoresis [4,5], magnetic-activated cell sorting (MACS) [5,6], and fluorescent activated cell sorting (FACS) [6]. FACS and MACS, in particular, which exploit characteristic differences between labeled and unlabeled cells, are frequently used in bio-MEMS. In FACS, target cells are marked with positive or negative charges using a laser or photomultiplier tube and then separated by electric fields. Similarly, in MACS, magnetic beads are used to mark and separate target living cells. Both methods are rather effective, but require immunolabeling of living cells, which will inevitably have an adverse effect on the cells. Furthermore, the immunolabeling procedures—pretreatment using a chemical dye, fluorescent or enzyme-linked immunoassays, and other specific molecular methods—all involve large costs and great complexity [7].

As an alternative, Pohl proposed dielectrophoresis (DEP), which exploits the motion of neutral but polarizable particles in nonuniform electric fields [8]. The origin of the DEP phenomenon lies in

Maxwell's electric stress tensor [9–12]: A spatially varying electric field induces unbalanced charges on the surfaces of living cells [11,13]. These unbalanced charges generate an electric stress tensor whose magnitude varies depending on the generalized permittivity of the cells. The net force developed is called the DEP force. The material properties of particles determine whether the DEP forces are positive or negative, as shown in Fig. 1. DEP-based devices exploit these net forces to separate target cells from other cells by exploiting small differences in generalized permittivity. But despite the many advantages and applications of DEP and related techniques, several practical issues remain unresolved.

To increase the cell separation efficiency of DEP-based devices, that is, to allow efficient separation of cells with small differences in their complex permittivity, it is important to find out optimal electrodes that generate physically reasonable nonuniform electric field [13]. Although other factors such as fluid velocity, fluid direction, and cell size also play important roles, their stochastic and chaotic nature prevent effective control [13]. Thus, it is our belief that optimizing the electric field distribution by controlling electrode shape is a practical and feasible method to maximize the cell separation efficiency of DEP-based devices.

In this research, to find out optimal electrodes and optimal electric field, we apply the topology optimization technology (one of the structural optimization technologies) which has been initiated to find out optimal mechanical structures [14]. Based on the optimization algorithm (sometimes called the mathematical programming), the topology optimization method can find out optimal structures maximizing or minimizing an object function subject to several constraints [15,16]. The method is widely used to

* Corresponding author.

E-mail addresses: ghy@knu.ac.kr, gilho.yoon@gmail.com (G.H. Yoon).

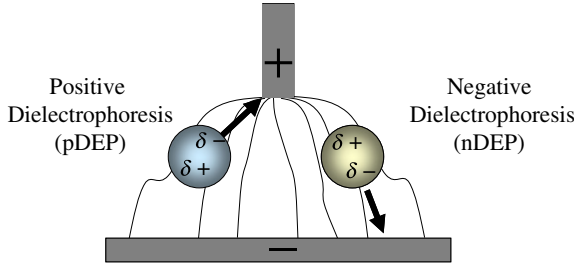


Fig. 1. Concept of DEP phenomena (pDEP: positive DEP and nDEP: negative DEP).

design machines and mechanical parts in the automotive, aerospace, and other industries [16–19] and it is now regarded as one of essential processes in industry. For an illustrative example of structural optimization, consider the problem in Fig. 2(a) having the left clamped boundary and a point downward load in a point of the right boundary. It has been an important problem in structural analysis society to design efficient and optimal structure sustaining given loads with limited materials [14,20–22]. After several major researches, it is now possible to mathematically optimize the member size (size optimization; Fig. 2(b)), optimize the profiles of existing design (shape optimization; Fig. 2(c)), and optimize the topology without the need for a given initial topology (topology optimization; Fig. 2(d)). As stated before, it is now common to use these structural optimization methods in classical mechanical engineering. But it is our finding that it is still rare to apply these methods to bio-MEMS [14,23–28]. Thus, in this paper, we explore the boundary of the structural optimization theory for bio-MEMS and expand the theory of topology optimization to design electrodes for DEP-based devices.

This paper is organized as follows. After describing the fundamentals of the DEP phenomenon, we implement an in-house-developed finite element code for solving the Laplace equation for the electric field inducing Maxwell's electric stress tensor. Furthermore, we investigate mathematical conditions for optimal electrodes, including interpolation functions for the material properties with respect to the design variable. After solving the formulated topology optimization problem, the optimized electrode shapes are presented. Finally, our findings, observations, and some possible topics for future research regarding bio-MEMS devices are summarized and discussed.

2. Statement of DEP phenomena

It is common to solve the full Maxwell's equations in general media for the strongly coupled electric and magnetic fields [29,30]. However, this mutual coupling can be ignored in DEP-based devices, reducing the full Maxwell's equations into the Laplace equation. From the calculated electric field from the Laplace equation, the integration of the simplified Maxwell's electric stress tensor exerted on a spherical cell or the DEP force can be obtained [25,31].

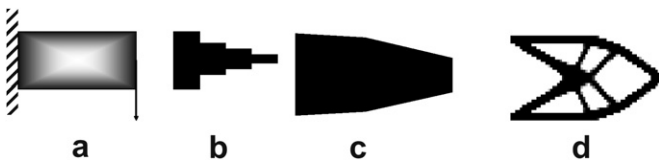


Fig. 2. Structural optimization: (a) the optimization problem, (b) size optimization, (c) shape optimization, and (d) topology optimization.

2.1. Simplified Maxwell's equation: Laplace equation

By ignoring the coupling between the electric and magnetic fields and assuming the irrotational electric field, the following Gauss and continuity equations can be derived for an isolated system, i.e., without connection to the outside environment.

$$\text{Gauss law : } \nabla_{\mathbf{x}} \cdot (\epsilon \mathbf{E}) = \rho \quad (1)$$

$$\text{Equation of continuity of charge : } -\nabla_{\mathbf{x}} \cdot (\sigma \mathbf{E}) = \frac{\partial \rho}{\partial t} \quad (2)$$

where the charge density is denoted by ρ . Without loss of generality, media have a spatially varying conductivity σ and permittivity ϵ .

$$\sigma = \sigma(\mathbf{x}), \quad \epsilon = \epsilon(\mathbf{x}) \quad (3)$$

where \mathbf{x} is the spatial position. By equating the differential of equation (1) with respect to time with equation (2), the following transient equation can be obtained.

$$\nabla_{\mathbf{x}} \cdot \left(\sigma \mathbf{E} + \frac{\partial}{\partial t} \epsilon \mathbf{E} \right) = 0 \quad \text{or} \quad \nabla_{\mathbf{x}} \cdot \left(\sigma \nabla_{\mathbf{x}} \phi + \frac{\partial}{\partial t} \epsilon \nabla_{\mathbf{x}} \phi \right) = 0 \quad (4)$$

where ϕ is a scalar electric potential. Therefore, to calculate DC or AC electric field in media, the transient system represented by equation (4) should be analytically or numerically solved. However, it is common to degenerate this transient system into a static equation with complex permittivity.

To proceed further, it is assumed that the electric field is frequency dependent. By employing a specific frequency ω and generalized permittivity ϵ^* , equation (4) can be simplified.

$$\nabla_{\mathbf{x}} \cdot (\epsilon^* \nabla_{\mathbf{x}} \phi) = 0 \quad \left(\epsilon^* = \epsilon - j \frac{\sigma}{\omega} \right) \quad (5)$$

In actual numerical computation, we use a real value for $\tilde{\epsilon}$ and not a complex value; the concept has been proven by many researches (see Ref. [29,32] and references therein). For example, if the electric field in a conductor is of interest, a very large value can be assigned to $\tilde{\epsilon}$. On the contrary, it is possible to use the permittivity of air or fluid to simulate the electric field inside media having a very small conductivity as follows:

$$\tilde{\epsilon} \gg \epsilon_{\text{fluid}} \quad \text{for conductor,} \quad \tilde{\epsilon} = \epsilon_{\text{fluid}} \quad \text{for media} \quad (6)$$

where the permittivity of media is ϵ_{fluid} . Many analysis methods can be employed to calculate the electric field in a given configuration with electrode, fluid, and particle. For a simple domain such as a box or a circle, an analytical solution for the electric field, the DEP force, and other associated quantities can be derived. However, numerical methods such as the finite volume

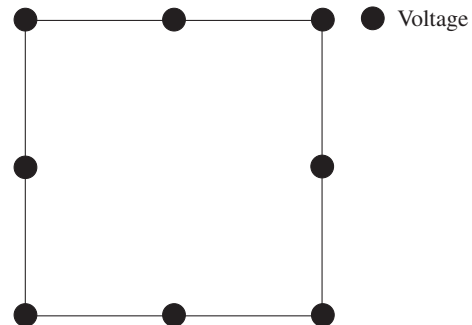


Fig. 3. The 8 node plane finite element for the electric potential equation (7).

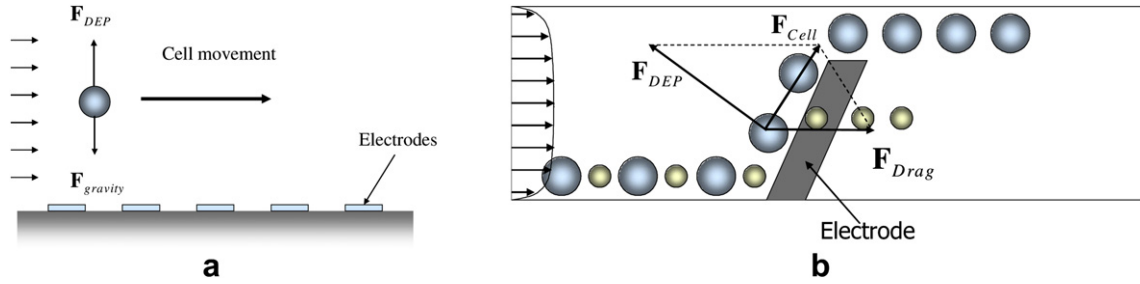


Fig. 4. Schematic of DEP devices. (a) A schematic of interdigitated electrode array and (b) a schematic of a 3D cell sorter.

method (FV method), finite difference method (FD method), and finite element method (FE method) should be used for general and complex configurations with modern computers and algorithms. In this paper, we rely on the FE method so that the structural optimization theory developed in the framework of the FE method can be easily incorporated.

Using the principle of virtual work, the following equation can be derived from equation (5).

$$\text{Electric potential equation : } \int (\nabla_{\mathbf{x}} \delta \phi)^T \cdot \tilde{\varepsilon}(\mathbf{x}) \nabla_{\mathbf{x}} \phi d\Omega = 0 \quad (7)$$

where the virtual voltage is denoted by $\delta \phi$. To solve the above weak formulation for the electric potential, the 8 node plane finite element shown in Fig. 3 is implemented in the framework of the MATLAB. The resulting linear equation can be stated.

$$\mathbf{K}(\tilde{\varepsilon}) \Phi = \mathbf{F} \quad (8)$$

$$\mathbf{K}(\tilde{\varepsilon}) = \sum_{e=1}^{NE} \mathbf{K}_e(\tilde{\varepsilon}_e) \quad (9)$$

$$\mathbf{K}_e = \int_{\Omega_e} \tilde{\varepsilon}_e \mathbf{B}^T \mathbf{B} d\Omega_e \quad (10)$$

where the global stiffness matrix, the e -th element stiffness matrix, and the potential gradient interpolation matrix are denoted by \mathbf{K} , \mathbf{K}_e , and \mathbf{B} , respectively. The global electric potential vector is Φ where the number of finite elements is NE and the permittivity of the e -th element is $\tilde{\varepsilon}_e$. (See Ref. [33] for more detail.)

2.2. DEP force

Any structure with permittivity $\varepsilon(\mathbf{x})$ in the electric field represented by equation (5) experiences an electrostatic force due to (electric) Maxwell' stress tensor, which is the symmetric 2-rank stress–momentum tensor of an electromagnetic field [29,30].

$$\mathbf{T}_e = \varepsilon(\mathbf{x}) \left(\mathbf{E} \mathbf{E} - \frac{\mathbf{E} \cdot \mathbf{E}}{2} \mathbf{I} \right) \quad (11)$$

This stress tensor generates a DEP force on polarized, but electrically neutral, cells inside the nonuniform electric field. Although the

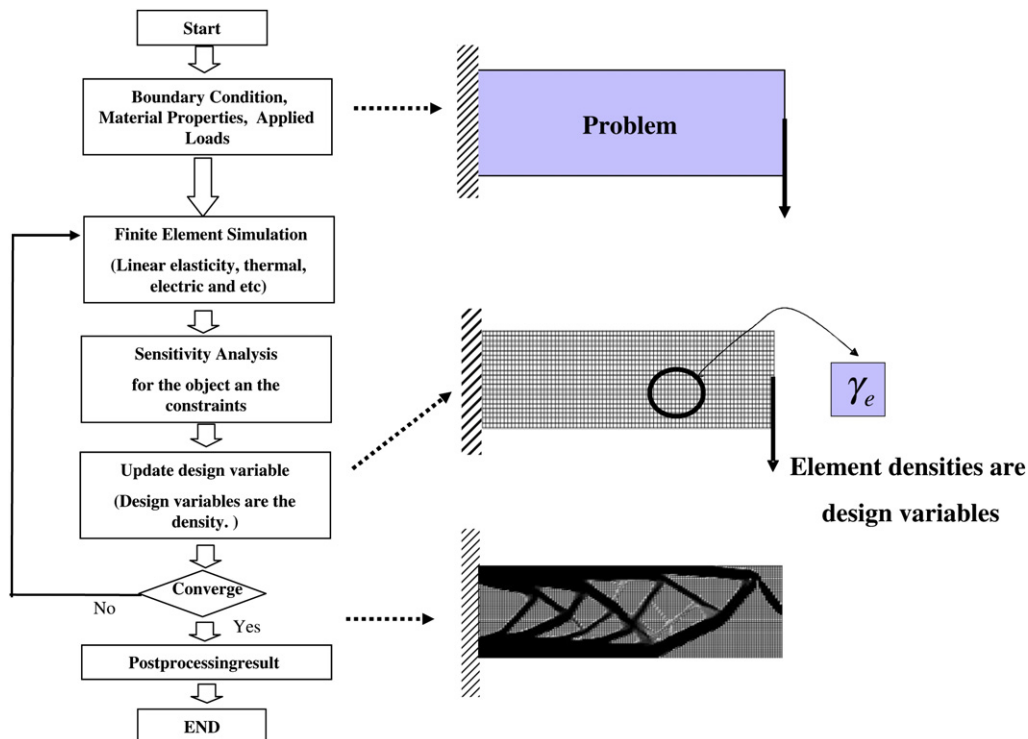


Fig. 5. The standard topology optimization process for a structural problem.

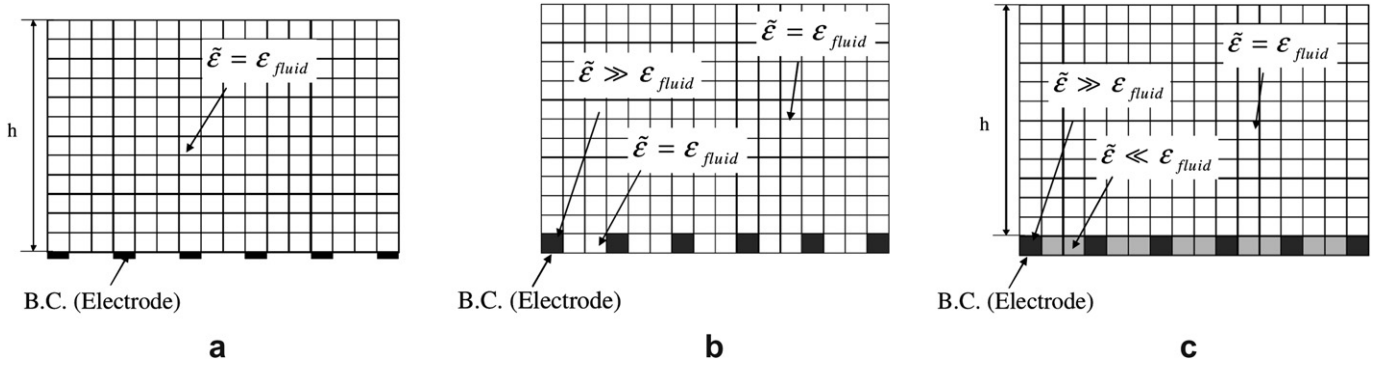


Fig. 6. The material models used for DEP. Black and white pixels represent $\gamma = 1$ and 0, respectively. (a) Domain of interest, (b) the first interpolation model, and (c) the second interpolation model used in topology optimization.

shape of the cell influences the electric field, it is complex and impractical to calculate the exact electric field inside media with several cells. So by assuming that the cell is small enough not to alter both the DC and the AC electric field and that the cell is a spherical particle of radius r suspended in a fluid of absolute dielectric permittivity ϵ_m , the average DEP force can be calculated as follows.

$$\mathbf{F}_{DEP} = 2\pi\epsilon_m r^3 \text{Re}(f_{CM}) \nabla |\mathbf{E}|^2 \quad (12)$$

where f_{CM} , the Clausius–Mossotti factor, is defined as follows

$$f_{CM} = \frac{\epsilon_p^* - \epsilon_m^*}{\epsilon_p^* + 2\epsilon_m^*} \left(\epsilon_p^* = \epsilon_p - j\frac{\sigma_p}{\omega}, \epsilon_m^* = \epsilon_m - j\frac{\sigma_m}{\omega} \right) \quad (13)$$

where the complex permittivities of the particle and its suspending medium are ϵ_p^* and ϵ_m^* , respectively. The square of the electric field gradient is defined as follows.

$$\nabla |\mathbf{E}|^2 = \frac{\partial}{\partial x} (E_x^2 + E_y^2) \mathbf{i} + \frac{\partial}{\partial y} (E_x^2 + E_y^2) \mathbf{j} \text{ in 2D} \quad (14)$$

$$\nabla |\mathbf{E}|^2 = \frac{\partial}{\partial x} (E_x^2 + E_y^2 + E_z^2) \mathbf{i} + \frac{\partial}{\partial y} (E_x^2 + E_y^2 + E_z^2) \mathbf{j} + \frac{\partial}{\partial z} (E_x^2 + E_y^2 + E_z^2) \mathbf{k} \text{ in 3D} \quad (15)$$

where the bases of the Cartesian coordinator are \mathbf{i}, \mathbf{j} , and \mathbf{k} . The electric fields of the directions X, Y , and Z are respectively denoted by E_x, E_y , and E_z . Further, derivations of equations (14) and (15) are possible:

$$\frac{\partial}{\partial x} (E_x^2 + E_y^2) = 2E_x E_{x,x} + 2E_y E_{y,x} \text{ in 2D} \quad (16-1)$$

$$\frac{\partial}{\partial y} (E_x^2 + E_y^2) = 2E_x E_{x,y} + 2E_y E_{y,y} \text{ in 2D} \quad (16-2)$$

$$\frac{\partial}{\partial x} (E_x^2 + E_y^2 + E_z^2) = 2E_x E_{x,x} + 2E_y E_{y,x} + 2E_z E_{z,x} \text{ in 3D} \quad (17-1)$$

$$\frac{\partial}{\partial y} (E_x^2 + E_y^2 + E_z^2) = 2E_x E_{x,y} + 2E_y E_{y,y} + 2E_z E_{z,y} \text{ in 3D} \quad (17-2)$$

$$\frac{\partial}{\partial z} (E_x^2 + E_y^2 + E_z^2) = 2E_x E_{x,z} + 2E_y E_{y,z} + 2E_z E_{z,z} \text{ in 3D} \quad (17-3)$$

Before proceeding further, the following observations can be made from equation (12), which represents the simplified DEP force.

1. The Clausius–Mossotti factor f_{CM} determines the direction of the DEP force. The direction of the DEP force changes with ϵ_p^* and ϵ_m^* .
2. The shape of the electrodes determines the value of the square of the electric field gradient. The factors in equation (12) besides $\nabla |\mathbf{E}|^2$ are dependent on the material properties and geometry of the cell. Therefore, in general, it is practical to control $\nabla |\mathbf{E}|^2$ in order to maximize the efficiency of DEP devices.

2.3. Observations on the movement of a particle suspended in a fluid

From the above observations, we can conclude that it is useful to optimize the electrode shape for DEP-based devices through structural optimization. Because the fluids inside microchannels often exhibit laminar flow, suspended cells experience a fluid drag force that linearly varies with the product of cross-sectional area and fluid velocity, as well as gravitational and DEP forces. Therefore, it is possible to predict the in-plane motion of cells using Navier–Stokes equation, as in Fig. 4. However, because the material properties and geometries of cells vary, in our opinion, it is better to consider the DEP force only. Furthermore, a more accurate calculation of the interaction between the fluid and cells would be very time consuming and chaotic.

3. Statement of topology optimization for DEP-based devices

In this section, we develop the necessary theory for topology optimization method for DEP-based devices. First, we describe the theory and introduce two material interpolation methods, which are necessary for topology optimization. Several analysis examples are considered to verify the validity of the developed theories.

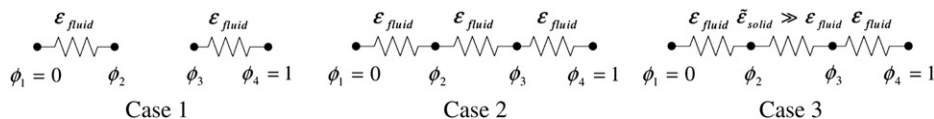


Fig. 7. Three 1D extreme models.

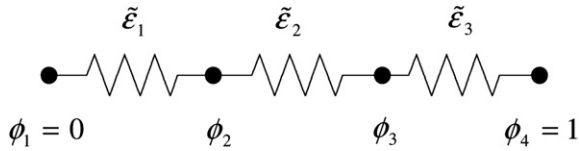


Fig. 8. A model using three 1D elements.

3.1. Topology optimization and material interpolation

Combined with size and shape optimization, topology optimization occupies a unique position in civil and mechanical engineering. In particular, the layouts of linear structures, whose

stiffness and mass matrices are independent of load and displacement, have been topologically optimized to maximize stiffness or reduce vibration or noise. (See Ref. [14] and references therein for more details.)

The goal of the topology optimization is to find out the optimal material distribution within a fixed design domain that maximizes or minimizes an objective function subject to several constraints. To evaluate an objective function and constraints in topology optimization, usually we employ the finite element procedure. And to model structural and nonstructural domains, a design variable which is used to interpolate material properties of finite element is assigned to each element; usually, a value of 1 and a small value is assigned to solid and void domains, respectively.

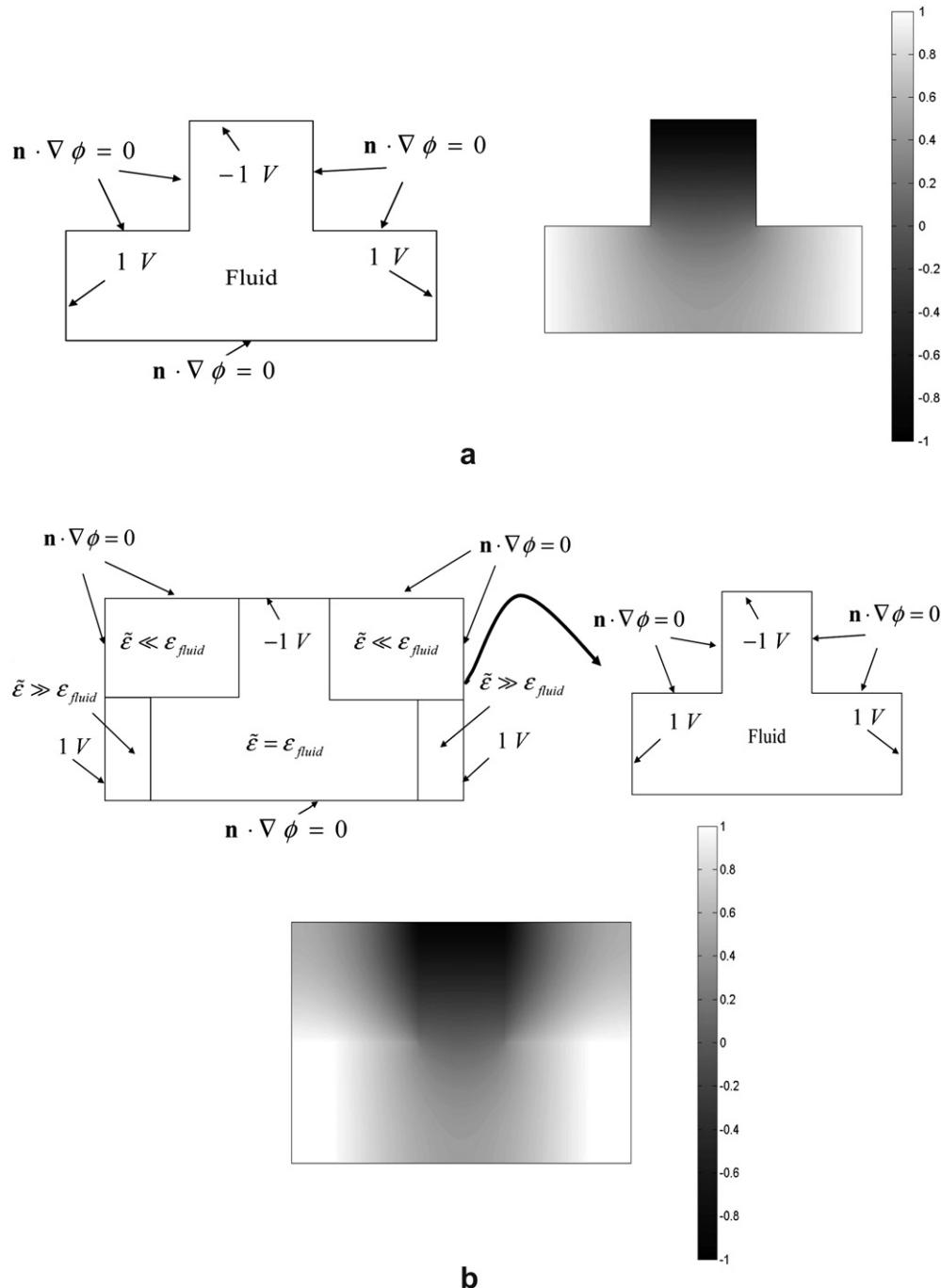


Fig. 9. Verification of the concept of topology optimization using the first material interpolation scheme.

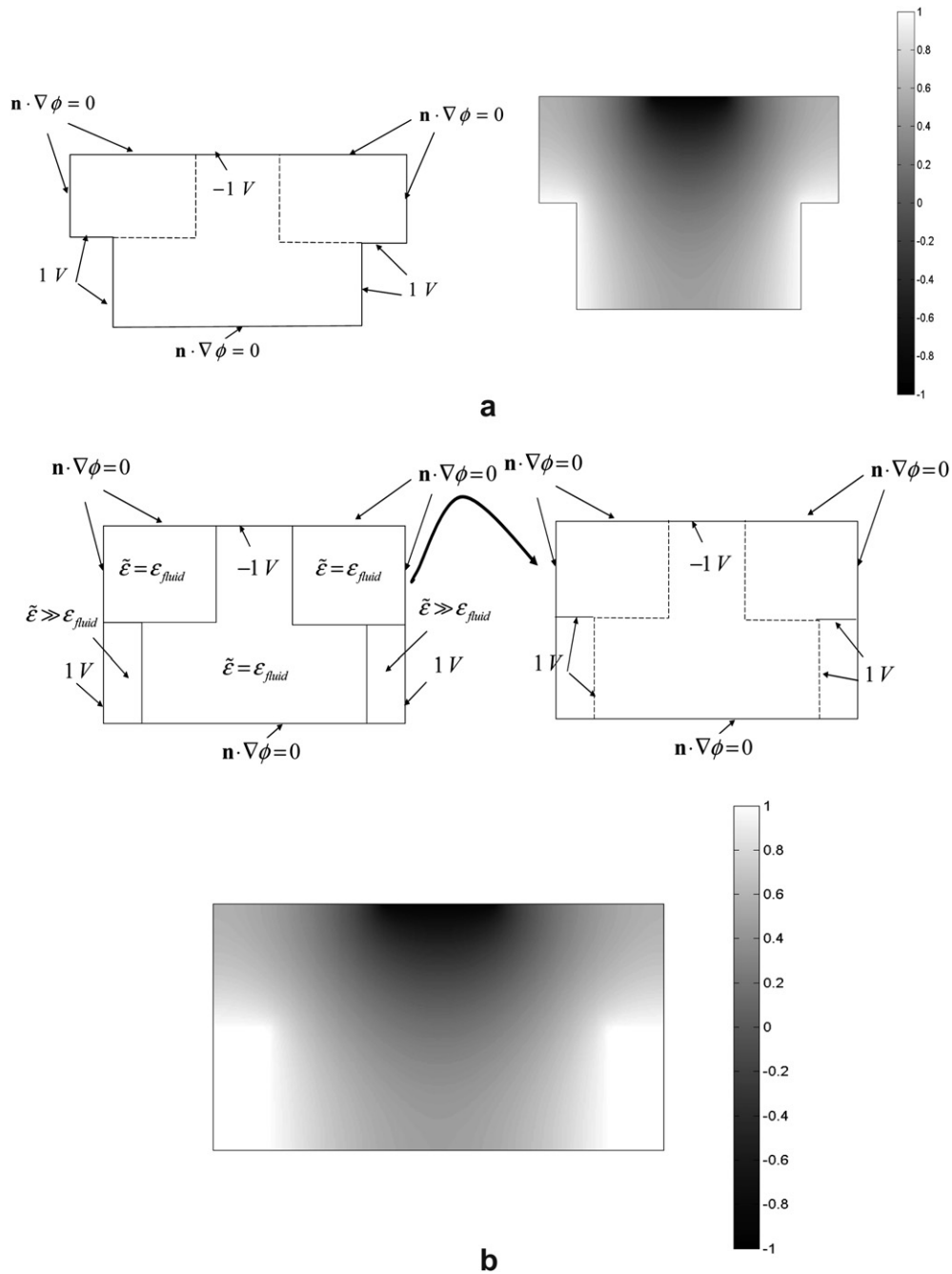


Fig. 10. Verification of the concept of topology optimization using the second material interpolation scheme.

Then the standard optimization algorithm, e.g., the algorithm shown in Fig. 5, is applied to find the optimal material distribution. This innovative idea has been validated by many researches on topology optimization (see Ref. [14] and the references therein). Furthermore, there are many studies that extend this concept to the development of new topology optimization schemes that are applied to new systems. (See Ref. [14] and the references therein).

As illustrated in Fig. 5, the material properties are interpolated with respect to the design variable assigned to each element. Therefore, it is an important issue to devise a proper material interpolation function with respect to the design variable. Before presenting the material interpolation function, the following points must be repeated.

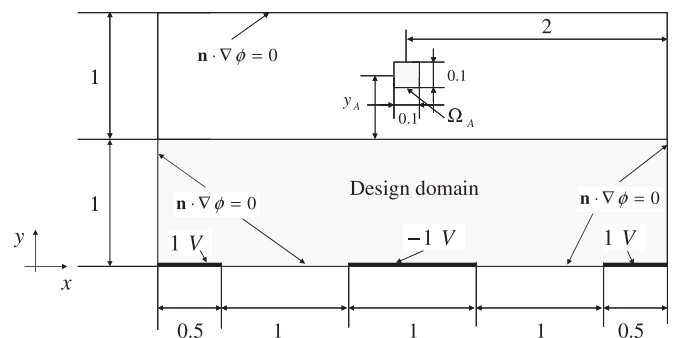


Fig. 11. Problem definition for 2D electrode design.

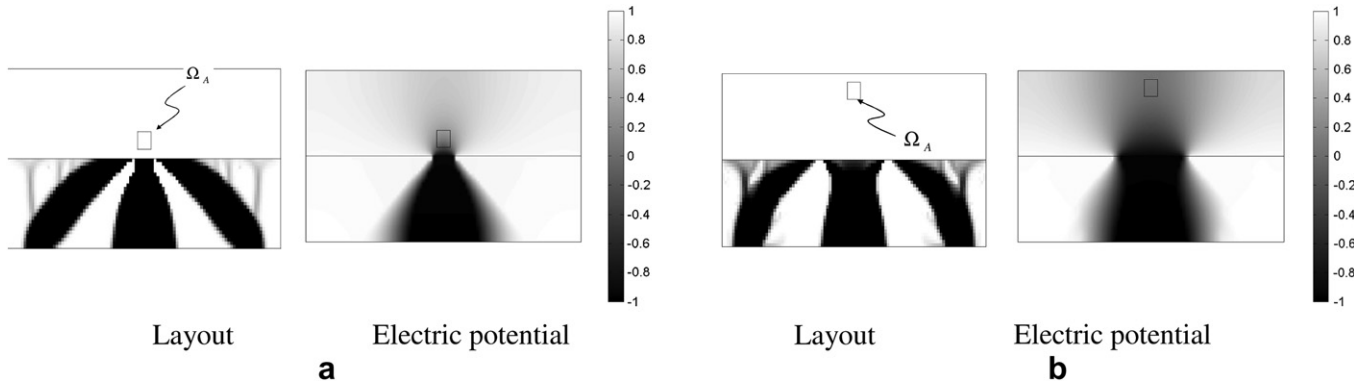


Fig. 12. Optimal layouts using the first material interpolation scheme (V^* : 50%, the relative permittivity of the fluid (ϵ_{fluid}): 1, the relative permittivity of the conductor (ϵ_{solid}): $10^3 \epsilon_{\text{fluid}}$). (a) An optimal layout for $y_A = 0.2$ and the electric field (objective: $-6.5064 \times 10^3 \text{ V}^2/\text{m}$), and (b) an optimal layout for $y_A = 0.8$ and the electric field (objective: $-46.62 \text{ V}^2/\text{m}$).

1. The square of the electric field gradient $|\nabla \mathbf{E}|^2$ is considered representative of the DEP force.
2. To control the electric field, the shape of the electrodes is optimized.
3. To calculate the electric field, the Laplace equation (5) is solved by the FE procedure. We assign large and small real values for the complex permittivity to simulate a perfect conductor and insulator, respectively.

After considering the above, the two material models for a DEP-based device are presented in this paper: the first material model (18) simulates a fluid and electrode submerged in it; the second (19) simulates an electrode and insulator. The physical differences between the materials are illustrated in Fig. 6; one of the main differences is that the physical domain for which the design variable is set to zero is different.

$$\text{Material Model 1 : } \tilde{\epsilon} = \begin{cases} \gamma = 1 : \tilde{\epsilon}_{\text{solid}} \gg \epsilon_{\text{fluid}} & \text{for electrode(perfect conductor)} \\ \gamma = 0 : \tilde{\epsilon}_{\text{void}} = \epsilon_{\text{fluid}} & \text{for fluid} \end{cases}, \quad (18)$$

$$\text{Material Model 2 : } \tilde{\epsilon} = \begin{cases} \gamma = 1 : \tilde{\epsilon}_{\text{solid}} \gg \epsilon_{\text{fluid}} & \text{for electrode(perfect conductor)} \\ \gamma = 0 : \tilde{\epsilon}_{\text{void}} \ll \epsilon_{\text{fluid}} & \text{for insulator} \end{cases}, \quad (19)$$

where $\tilde{\epsilon}_{\text{solid}}$ and $\tilde{\epsilon}_{\text{void}}$ are the upper and the low limit of the permittivity used in the Laplace equation, respectively. The design variable is denoted by γ . Note that 1 and 0 are assigned to γ for solid and void domains, respectively.

Using these two material models, a discrete design optimization problem is defined to find the optimal distributions of $\tilde{\epsilon}_{\text{solid}}$ and $\tilde{\epsilon}_{\text{void}}$ inside the design domain:

$$\begin{aligned} & \text{Min } f(\gamma) \\ & \gamma \in [0, 1] \\ & \text{S.t. } g_i(\gamma) \leq 0 \quad i = 1, 2, \dots, \text{nc} (\text{nc : the number of constraints}) \end{aligned} \quad (20)$$

where f and g_i are the objective function and the i th constraint, respectively; the detailed functional forms of equation (20) are presented later (section 4). It is possible to solve the discrete optimization problem using an evolving algorithm such as a genetic algorithm and

simulated annealing. However, the discrete design optimization problem is known to be a difficult problem to solve: the difficulties in the discrete topology optimization problem are attributed to the difficulties of nonconvex optimization and heavy computational loads. Therefore, it is common to relax this discrete design optimization problem using a continuous variable as follows [14,29]:

$$\begin{aligned} & \text{Min } f(\gamma) \\ & \text{S.t. } g_i(\gamma) \leq 0 \quad i = 1, 2, \dots, \text{nc} \end{aligned} \quad (21)$$

$$0 \leq \gamma \leq 1 \quad (22)$$

By using a continuous design variable, the material properties can also be relaxed. A popular relaxation method is density based method (sometimes called the SIMP (Solid Isotropic Material with Penalization) for structural problems), which interpolates the two discrete design variable values using a polynomial function as follows.

$$\tilde{\epsilon} = \begin{cases} \tilde{\epsilon}_{\text{solid}} \tilde{\epsilon}_{\text{void}} \rightarrow \tilde{\epsilon}(\gamma) = (\tilde{\epsilon}_{\text{solid}} - \tilde{\epsilon}_{\text{void}}) \gamma^n + \tilde{\epsilon}_{\text{void}}, 0 = \gamma_{\min} \leq \gamma \leq 1 \end{cases} \quad (23)$$

where the design variable γ varies from a very small value, γ_{\min} , to 1. The permittivity varies from $\tilde{\epsilon}_{\text{void}}$ to $\tilde{\epsilon}_{\text{solid}}$, and n is the penalty. It is common to use a real value from 2 to 4 as the penalty factor [14,29]. In this paper, several empirical tests are performed to choose a proper penalty factor. And because the constant penalty factor, 2, provides reasonable results, we use this value for all numerical examples unless stated otherwise.

3.2. Analysis examples

To verify the concept of topology optimization discussed above, this section provides several numerical examples.

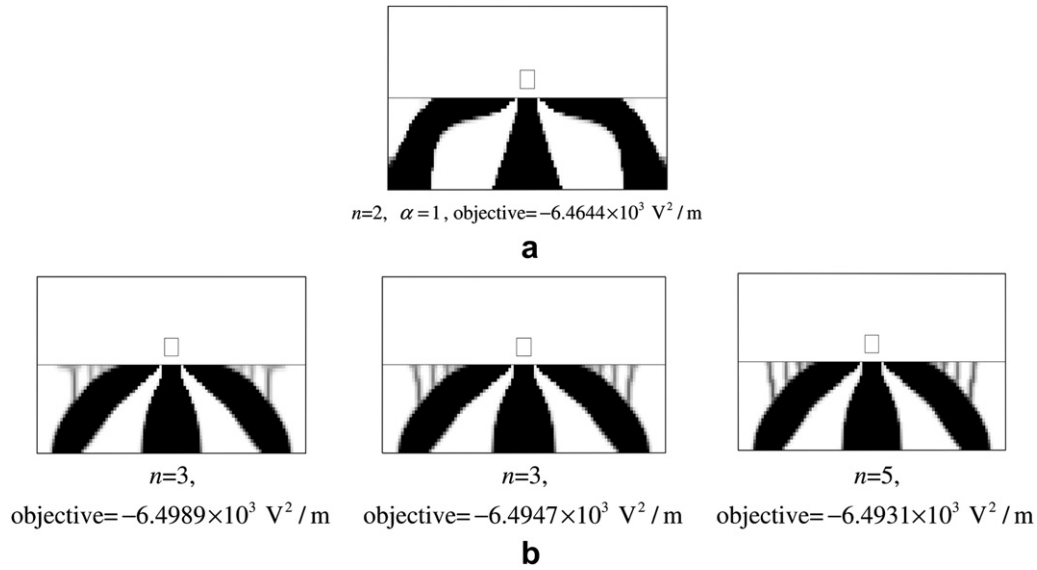


Fig. 13. Numerical tests for the gray elements. (a) optimized layouts with the explicit penalty ($\alpha\gamma(1-\gamma)$) and (b) Optimized layouts with various implicit penalties.

3.2.1. 1D example

Here, three simple models having unit length, unit area, and fluid permittivity $\varepsilon_{\text{fluid}}$ are simulated in Fig. 7. Although in the standard FE procedure, the three models are independently modeled, in topology optimization method, the single FE model shown in Fig. 8 is employed to simulate all the three; just material properties—in this case, permittivity—is changed. The potentials of the second and the third nodes can be calculated as follows for each model.

Case 1: $\phi_2 = 0 \text{ V}$ and $\phi_3 = 1 \text{ V}$

Case 2: $\phi_2 = 1/3 \text{ V}$ and $\phi_3 = 2/3 \text{ V}$

Case 3: $\phi_2 = 1/2 \text{ V}$ and $\phi_3 = 1/2 \text{ V}$

In the model shown in Fig. 8, the permittivities of the first, second, and third elements are denoted by $\tilde{\varepsilon}_1, \tilde{\varepsilon}_2$, and $\tilde{\varepsilon}_3$, respectively.

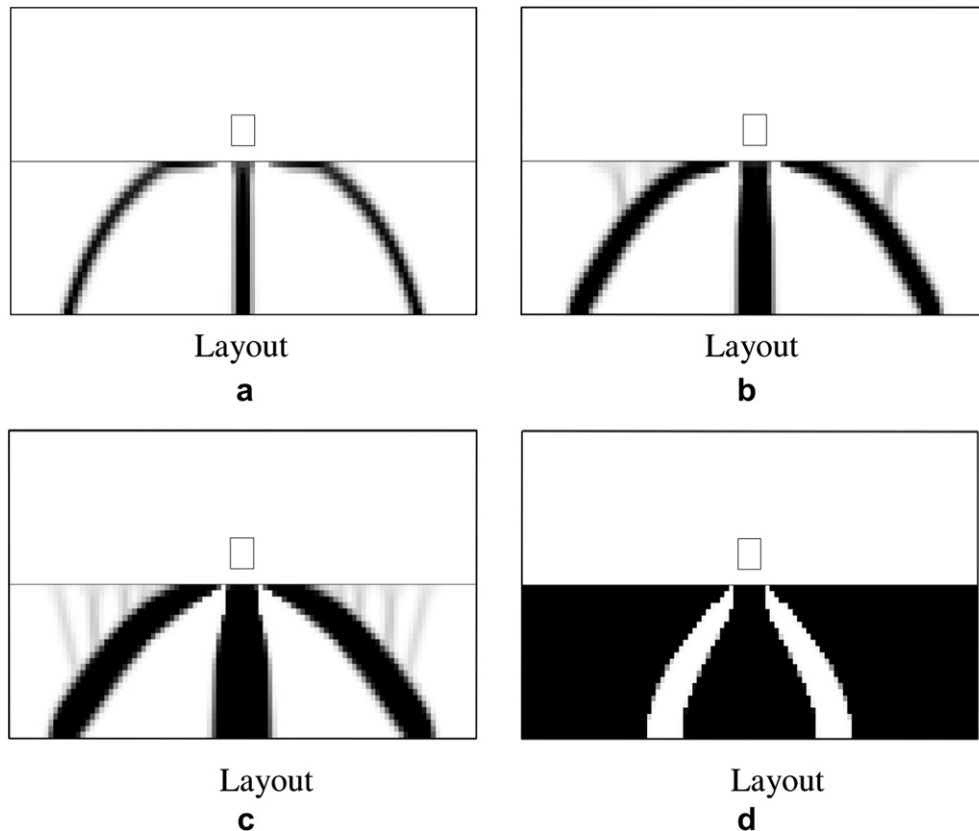


Fig. 14. Optimal layouts with different material usages. (a) V^* : 10%, objective: $-5.27 \times 10^3 \text{ V}^2/\text{m}$, (b) V^* : 20% V^s : 10%, objective: $-5.34 \times 10^3 \text{ V}^2/\text{m}$, (c) V^* : 30%, objective: $-6.30 \times 10^3 \text{ V}^2/\text{m}$, and (d) V^* : 100%, objective: $-6.59 \times 10^3 \text{ V}^2/\text{m}$, (Volume usage = 86.94%).

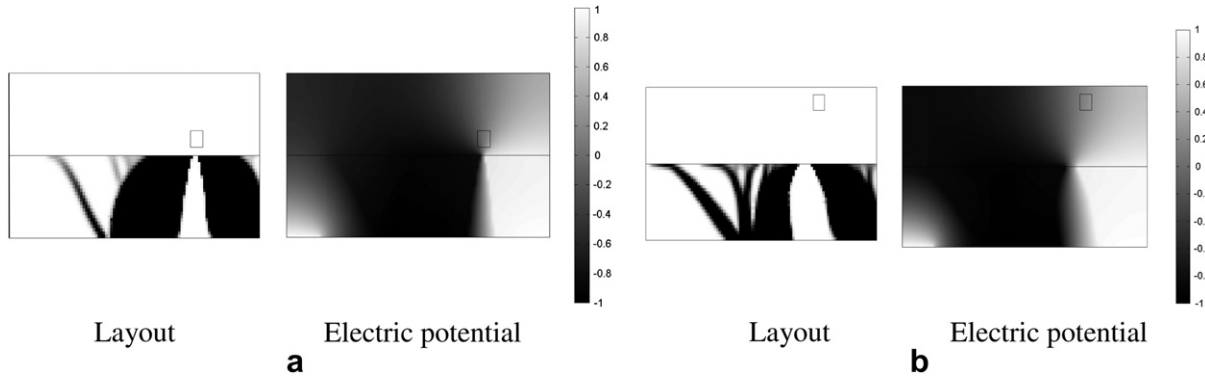


Fig. 15. Optimal layouts for the different actuation area. (a) An optimal layout $y_A = 0.2$ and the corresponding electric field (objective: $-4.15 \times 10^3 \text{ V}^2/\text{m}$), and (b) an optimal layout $y_A = 0.8$ and the corresponding electric field (objective: $-32.37 \times 10^3 \text{ V}^2/\text{m}$).

Because the elements have unit area and length, the system matrix can be constructed as follows.

$$\begin{bmatrix} \tilde{\epsilon}_1 & -\tilde{\epsilon}_1 & 0 & 0 \\ -\tilde{\epsilon}_1 & \tilde{\epsilon}_1 + \tilde{\epsilon}_2 & -\tilde{\epsilon}_2 & 0 \\ 0 & -\tilde{\epsilon}_2 & \tilde{\epsilon}_2 + \tilde{\epsilon}_3 & -\tilde{\epsilon}_3 \\ 0 & 0 & -\tilde{\epsilon}_3 & \tilde{\epsilon}_3 \end{bmatrix} \begin{bmatrix} \phi_1 \\ \phi_2 \\ \phi_3 \\ \phi_4 \end{bmatrix} = \begin{bmatrix} 0 \\ 0 \\ 0 \\ 0 \end{bmatrix} \quad (24)$$

After applying the boundary conditions, the potentials of the second and the third nodes can be computed.

$$\phi_2 = \frac{\tilde{\epsilon}_1(\tilde{\epsilon}_2 + \tilde{\epsilon}_3)\phi_1 + \tilde{\epsilon}_2\tilde{\epsilon}_3\phi_4}{(\tilde{\epsilon}_1\tilde{\epsilon}_2 + \tilde{\epsilon}_1\tilde{\epsilon}_3 + \tilde{\epsilon}_2\tilde{\epsilon}_3)} \quad (25)$$

$$\phi_3 = \frac{\tilde{\epsilon}_1\tilde{\epsilon}_2\phi_1 + \tilde{\epsilon}_3(\tilde{\epsilon}_1 + \tilde{\epsilon}_2)\phi_4}{(\tilde{\epsilon}_1\tilde{\epsilon}_2 + \tilde{\epsilon}_1\tilde{\epsilon}_3 + \tilde{\epsilon}_2\tilde{\epsilon}_3)} \quad (26)$$

Then, for the above three models, the permittivities of the first and the third elements are set to ϵ_{fluid} and the pseudo-permittivity of the second element, $\tilde{\epsilon}_2$, is assigned.

$$\phi_2 = \frac{\epsilon_{\text{fluid}}(\tilde{\epsilon}_2 + \epsilon_{\text{fluid}})\phi_1 + \tilde{\epsilon}_2\epsilon_{\text{fluid}}\phi_4}{(2\epsilon_{\text{fluid}}\tilde{\epsilon}_2 + \epsilon_{\text{fluid}}^2)} \quad (27)$$

$$\phi_3 = \frac{\epsilon_{\text{fluid}}\tilde{\epsilon}_2\phi_1 + \epsilon_{\text{fluid}}(\epsilon_{\text{fluid}} + \tilde{\epsilon}_2)\phi_4}{(2\epsilon_{\text{fluid}}\tilde{\epsilon}_2 + \epsilon_{\text{fluid}}^2)} \quad (28)$$

To model the case 1, the second element is modeled as an insulator; $\tilde{\epsilon}_2$ can be set to a very small value ($\tilde{\epsilon}_2 \ll \epsilon_{\text{fluid}}$). Therefore, the following asymptotic behaviors can be obtained.

$$\tilde{\epsilon}_2 \ll \epsilon_{\text{fluid}} (\text{Insulator}) : \phi_2 \rightarrow \phi_1, \phi_3 \rightarrow \phi_4 \quad (29)$$

To model the case 2, it is obvious that $\tilde{\epsilon}_2$ can be set to ϵ_{fluid} and the potentials of the two nodes are calculated as follows.

$$\tilde{\epsilon}_2 = \epsilon_{\text{fluid}} (\text{Fluid}) : \phi_2 = \frac{2\phi_1 + \phi_4}{3}, \phi_3 = \frac{\phi_1 + 2\phi_4}{3} \quad (30)$$

Similar to the previous cases, $\tilde{\epsilon}_2$ is set to a very high value, i.e., $\tilde{\epsilon}_2 \gg \epsilon_{\text{fluid}}$. The potentials of the two nodes are calculated as follows.

$$\tilde{\epsilon}_2 \gg \epsilon_{\text{fluid}} (\text{Conductor}) : \phi_2 \rightarrow 1/2 \text{ V}, \phi_3 \rightarrow 1/2 \text{ V} \quad (31)$$

As shown here, it is possible to simulate the three 1D models by changing the material properties of the second element. What we should emphasize here is that in principle, $\tilde{\epsilon}_2$ should be infinity for a perfect conductor, which is impossible for a computer algorithm. From several numerical tests, it is found that a value 1000 times larger value than ϵ_{fluid} is sufficient to simulate a perfect conductor in terms of the electric field. Therefore, unless stated otherwise, a value of $1000\epsilon_{\text{fluid}}$ is used in this paper.

3.2.2. 2D example

For the second example, the two dimensional domains presented in Figs. 9 and 10 are considered. First, to simulate the model in Fig. 9(a), the model is embedded in the larger domain shown in

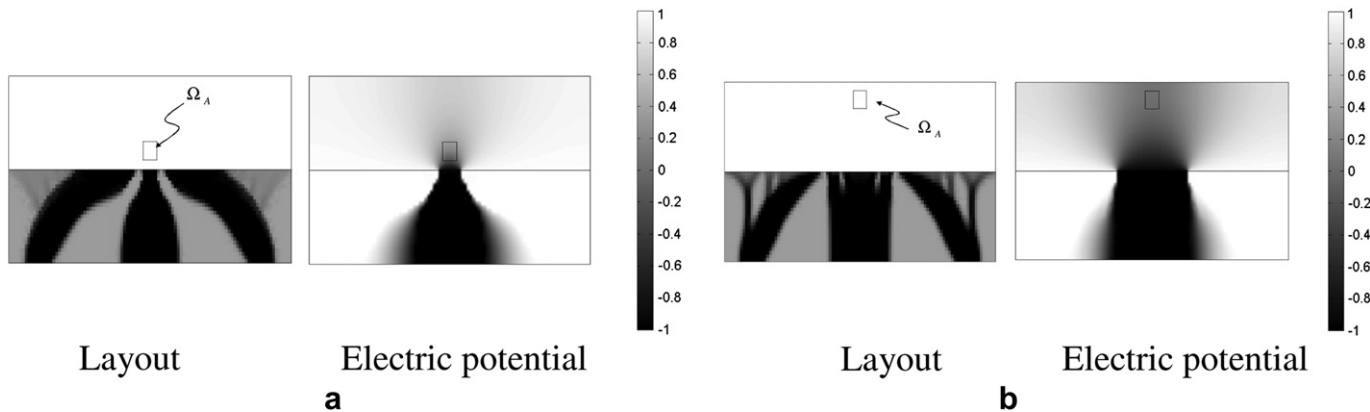


Fig. 16. Optimal layouts using the second material interpolation scheme (V^* : 50%, the relative permittivity of the fluid (ϵ_{fluid}): 1, the relative permittivity of the insulator (ϵ_{void}): $10^{-6}\epsilon_{\text{fluid}}$, the relative permittivity of the conductor (ϵ_{solid}): $10^3\epsilon_{\text{fluid}}$). (a) An optimal layout for $y_A = 0.2$ and the electric field (objective: $-6.99 \times 10^3 \text{ V}^2/\text{m}$), and (b) an optimal layout for $y_A = 0.8$ and the electric field (objective: $-47.76 \text{ V}^2/\text{m}$).

problems. For a stable optimization algorithm, the method of moving asymptotes (MMA) is employed, but other optimization algorithms can also be incorporated [34].

4.1. Example 1

In the optimization problem of equation (32), the objective is maximization of the y -directional DEP force using a limited amount of material. The design domain is a 4×2 rectangular box discretized by 100×50 quad elements. The boundary conditions and the material properties are arbitrarily chosen for the purpose of illustration and depicted in Fig. 11. By solving the optimization problem, we obtain the optimal electrode layouts maximizing the y -directional DEP force.

$$\begin{aligned} & \text{Max} \int_{\Omega_A} \frac{\partial}{\partial y} (E_x^2 + E_y^2) d\Omega \\ & \text{S.t.} \int_{\Omega_d} \gamma d\Omega \leq V^* \quad (0 \leq \gamma \leq 1; V^* : \text{the volume limit}), \end{aligned} \quad (32)$$

where the actuation area and the design domain are denoted by Ω_A and Ω_d , respectively. First, we employ the first material interpolation (fluid–conductor) scheme (18), i.e., 0 and 1 indicate fluid and conductor, respectively. Fig. 12 shows the optimization results with two different actuation areas, e.g., 0.2 m and 0.8 m for y_A . Optimal electrode configurations that maximize the y -directional DEP force are generated. One interesting physical characteristic is that the gap between the electrodes is reduced when the actuation area is closer to the electrodes.

From the above results, we could observe the gray elements. Unlike in the elasticity problem, it is not clear how to interpret these gray elements from the physical point of view. Furthermore for the purpose of the post processing, it is better to have the clear black and white results. For these reasons, in Fig. 13, we tested several implicit penalties of n and the explicit penalty $\alpha\gamma(1 - \gamma)$ to the objective function. Unlike in the elasticity problem, the implicit penalties are not so much effective to remove the gray elements whereas the explicit penalty provides the clearly converged black and white results.

Because MEMS electrodes are commonly created by etching, the mass constraint is actually not necessary. However, it is common to use this constraint in topology optimization; hence, equation (32) is employed. The mass constraint in equation (32) means that the ratio of the area of black domains over the area of design domains in the figures is controlled. (See Ref. [14] for the explanation of the mass constraint.) Fig. 14 shows results with different material usages using this constraint (29). As shown, the overall layouts are similar to each other. Two curled anode electrodes and a straight cathode appear. Furthermore, with 100% volume usage, where the optimization formulation of (32) is unconstrained, the optimization algorithm automatically determines the optimal mass usage (about 86% in this example) to generate the gaps between the electrodes.

To consider more complex situations, an optimization problem with another different actuation area located at the right of the domain (marked by the small rectangular box) is considered (Fig. 15). Unlike in the previous example, it is not easy to graphically represent the optimal layouts. An interesting feature is that branches appear from the center to the left to block the effect of the left electrode having 1 V. In our opinion, these kinds of designs are not intuitive.

For the next example, we solve this problem again using the second material interpolation scheme (insulator–conductor; Fig. 16). Here, the gray domain in has a very low permittivity ($\epsilon_{\text{flu-id}} \times 10^{-6}$) to simulate an insulator. Compared with the results

obtained using the first interpolation function (fluid–conductor), differences in the details of the layouts can be seen.

4.2. Example 2

Because the design domain and the boundary conditions of the first example are relatively simple, only small differences appear in the layouts obtained using the two different material interpolation schemes, as observed in Figs. 12 and 16. To see more dramatic differences, we consider the design problem shown in Fig. 17, that is, to maximize the x -direction DEP force. The boundary conditions, the actuation area, and the design domain are arbitrarily chosen. Fig. 17(b) and (c) shows the obtained results for the first and the second material interpolation models, respectively. As shown, unlike in the first numerical example, there are significant differences in the layouts. Furthermore, the obtained optimal layouts are the designs that are hard to obtain simply by engineer's intuition.

$$\begin{aligned} & \text{Max} \int_{\Omega_A} \frac{\partial}{\partial x} (E_x^2 + E_y^2) d\Omega \\ & \text{S.t.} \int_{\Omega_d} \gamma d\Omega \leq V^* \quad (0 \leq \gamma \leq 1) \end{aligned} \quad (33)$$

5. Conclusions

This paper presents a new topology optimization procedure for electrodes in DEP-based devices. The DEP force depends on the shape of the electrodes and hence it is important to optimize the electrode layout. To our knowledge, only heuristic design processes have been applied to electrode design thus far. Therefore, we explored the possibility of applying a structural optimization scheme called topology optimization. The proposed method, instead of using heuristics, relies on an optimization algorithm (sometimes called mathematical programming) find optimal topologies. For this, the Laplace equation is solved with appropriate boundary conditions to evaluate the potential field in design domains. The spatial derivative of the square of the electric field is considered as the objective function. By setting the material property distribution, optimal layouts that are physically realizable can be obtained. It was also found that there are the two possible material interpolation functions. By assigning a permittivity value equal to that of the fluid medium to the void regions, the void regions could be regarded as media. On the other hand, it is also possible to assign a very low permittivity to simulate the Neumann boundary condition at the boundaries of void regions. Depending on the material interpolation function selected, different optimal layouts were obtained.

In conclusion, the structural optimization method mainly developed for structural problems can be used as a basis for designing bio-MEMS devices. As future work, topology optimization for controlling the electric field distribution is being explored.

Acknowledgement

The authors acknowledge the support from Basic Science Research Program through the National Research Foundation of Korea (NRF) funded by the Ministry of Education, Science and Technology (2009-0087705) (GHY), from the Grant of the Korean Ministry of Education, Science and Technology (The Regional Core Research Program/Anti-aging and Well-being Research Center) (GHY) and from the Pioneer Research Center Program “Bacteriobot” through the National Research Foundation of Korea funded by the Ministry of Education, Science and Technology (2009-0082953). (JYP)

References

- [1] P.R.C. Gascoyne, J.V. Vykoukal, Dielectrophoresis-based sample handling in general-purpose programmable diagnostic instruments, *Proceedings of the IEEE* 92 (2004) 22–42.
- [2] P. Gascoyne, C. Mahidol, M. Ruchirawat, J. Satayavivad, P. Watcharasi, F.F. Becker, Microsample preparation by dielectrophoresis: isolation of malaria, *Lab on a Chip* 2 (2002) 70–75.
- [3] S.L. Friedman, F.J. Roll, Isolation and culture of hepatic lipocytes, Kupffer cells, and sinusoidal endothelial cells by density gradient centrifugation with Stratan, *Analytical Biochemistry* 161 (1987) 207–218.
- [4] A. Tulp, D. Verwoerd, J. Pieters, Application of an improved density gradient electrophoresis apparatus to the separation of proteins, cells and subcellular organelles, *Electrophoresis* 14 (1993) 1295–1301.
- [5] S. Miltenyi, W. Muller, W. Weichel, A. Radbruch, High gradient magnetic cell separation with MACS, *Cytometry* 11 (1990) 231–238.
- [6] P. Malatesta, E. Hartfuss, M. Gotz, Isolation of radial glial cells by fluorescent-activated cell sorting reveals a neuronal lineage, *Development* 127 (2000) 5253–5263.
- [7] C.M. Das, F. Becker, S. Vernon, J. Noshari, C. Joyce, P.R. Gascoyne, Dielectrophoretic segregation of different human cell types on microscope slides, *Analytical Chemistry* 77 (2005) 2708–2719.
- [8] H.A. Pohl, *Dielectrophoresis: The Behavior of Neutral Matter in Non-uniform Electric Fields*, Cambridge University Press, Cambridge, UK, 1978.
- [9] S.W. Lee, J.H. Choi, Y.K. Kim, Analysis and experimental investigation of dielectrophoretic force in a planar electrode structure, *Journal of Micromechanics and Microengineering* 6 (1996) 66–68.
- [10] L.C. Hsiung, C.H. Yang, C.L. Chiu, C.L. Chen, Y. Wang, H. Lee, J.Y. Cheng, M.C. Ho, A.M. Wo, A planar interdigitated ring electrode array via dielectrophoresis for uniform patterning of cells, *Biosensors & Bioelectronics* 24 (2008) 869–875.
- [11] T. Sun, N.G. Green, H. Morgan, Analytical solutions for the electric field and dielectrophoretic force in a dielectrophoretic focusing electrode structure, *Applied Physics Letters* 92 (2008).
- [12] M. Dimaki, P. Boggild, Dielectrophoresis of carbon nanotubes using micro-electrodes: a numerical study, *Nanotechnology* 15 (2004) 1095–1102.
- [13] J. Park, B. Kim, S.K. Choi, S. Hong, S.H. Lee, K.I. Lee, An efficient cell separation system using 3D-asymmetric microelectrodes, *Lab on a Chip* 5 (2005) 1264–1270.
- [14] M.P. Bendsoe, O. Sigmund, *Topology Optimization Theory, Methods and Applications*, Springer-Verlag, New York, 2003.
- [15] G.H. Yoon, J.S. Jensen, O. Sigmund, Topology optimization of acoustic-structure interaction problems using a mixed finite element formulation, *International Journal for Numerical Methods in Engineering* 70 (2007) 1049–1075.
- [16] J. Yoo, N. Kikuchi, Topology optimization in magnetic fields using the homogenization design method, *International Journal for Numerical Methods in Engineering* 48 (2000) 1463–1479.
- [17] J.H. Rong, Y.M. Xie, X.Y. Yang, Q.Q. Liang, Topology optimization of structures under dynamic response constraints, *Journal of Sound and Vibration* 234 (2000) 177–189.
- [18] S. Canfield, M. Frecker, Topology optimization of compliant mechanical amplifiers for piezoelectric actuators, *Structural and Multidisciplinary Optimization* 20 (2000) 269–279.
- [19] D. Inoyama, B.P. Sanders, J.J. Joo, Topology optimization approach for the determination of the multiple-configuration morphing wing structure, *Journal of Aircraft* 45 (2008) 1853–1862.
- [20] C.S. Andreasen, A.R. Gersborg, O. Sigmund, Topology optimization of micro-fluidic mixers, *International Journal for Numerical Methods in Fluids* 61 (2009) 498–513.
- [21] S. Nishiwaki, T. Nomura, S. Kinoshita, K. Izui, M. Yoshimura, K. Sato, K. Hirayama, Topology optimization for cross-section designs of electromagnetic waveguides targeting guiding characteristics, *Finite Elements in Analysis and Design* 45 (2009) 944–957.
- [22] M.M. Gregersen, F. Okkels, M.Z. Bazant, H. Bruus, Topology and shape optimization of induced-charge electro-osmotic micropumps, *New Journal of Physics* 11 (2009).
- [23] W.J. Ye, S. Mukherjee, N.C. MacDonald, Optimal shape design of an electrostatic comb drive in microelectromechanical systems, *Journal of Microelectromechanical Systems* 7 (1998) 16–26.
- [24] J.T.Y. Lin, J.T.W. Yeow, Enhancing dielectrophoresis effect through novel electrode geometry, *Biomedical Microdevices* 9 (2007) 823–831.
- [25] A. Al-Jarro, J. Paul, D.W.P. Thomas, J. Crowe, N. Sawyer, F.R.A. Rose, K.M. Shakesheff, Direct calculation of Maxwell stress tensor for accurate trajectory prediction during DEP for 2D and 3D structures, *Journal of Physics D-Applied Physics* 40 (2007) 71–77.
- [26] J.H. Kuang, C.J. Chen, The nonlinear electrostatic behavior for shaped electrode actuators, *International Journal of Mechanical Sciences* 47 (2005) 1172–1190.
- [27] W.J. Ye, S. Mukherjee, Optimal shape design of three-dimensional MEMS with applications to electrostatic comb drives, *International Journal for Numerical Methods in Engineering* 45 (1999) 175–194.
- [28] B.D. Jensen, S. Mutlu, S. Miller, K. Kurabayashi, J.J. Allen, Shaped comb fingers for tailored electromechanical restoring force, *Journal of Microelectromechanical Systems* 12 (2003) 373–383.
- [29] G.H. Yoon, O. Sigmund, A monolithic approach for topology optimization of electrostatically actuated devices, *Computer Methods in Applied Mechanics and Engineering* 197 (2008) 4062–4075.
- [30] E. Lemaire, V. Rochus, J.C. Golinval, P. Duysinx, Microbeam pull-in voltage topology optimization including material deposition constraint, *Computer Methods in Applied Mechanics and Engineering* 197 (2008) 4040–4050.
- [31] X.J. Wang, X.B. Wang, P.R.C. Gascoyne, General expressions for dielectrophoretic force and electrorotational torque derived using the Maxwell stress tensor method, *Journal of Electrostatics* 39 (1997) 277–295.
- [32] D.K. Cheng, *Field and Wave Electromagnetics*, Addison-Wesley, New York, 1989.
- [33] K.J. Bathe, *Finite Element Procedures*, Prentice Hall, New Jersey, 1996.
- [34] K. Svanberg, The method of moving asymptotes—a new method for structural optimization, *International Journal for Numerical Methods in Engineering* 24 (1987) 359–373.